to non-alcoholic fatty liver disease, which not only strongly affects the pathophysiology of type 2 diabetes, but also cardiovascular disease, and hepatic and extrahepatic cancers.[8] A more detailed substratification with the use of the adipokine adiponectin and the hepatokine fetuin-A as parameters in cluster analyses allowed separation of insulin resistance associated with visceral adiposity from insulin resistance associated with non-alcoholic fatty liver disease.[9] We believe that a sequential risk stratification approach should be applied in future studies. This procedure could include the initial use of an established risk stratification method, (eg, involving cluster analysis with clinically available routine parameters), followed by more precise phenotyping methods, which would allow identification of subclusters.

We declare no competing interests.

*Norbert Stefan, Matthias B Schulze
norbert.stefan@med.uni-tuebingen.de

Department of Internal Medicine IV, University Hospital Tübingen, Tübingen 72076, Germany (NS); Institute of Diabetes Research and Metabolic Diseases of the Helmholtz Centre Munich, Tübingen, Germany (NS); German Center for Diabetes Research, Neuherberg, Germany (NS, MBS); Department of Molecular Epidemiology, German Institute of Human Nutrition Potsdam-Rehbruecke, Nuthetal, Germany (MBS); Institute of Nutritional Science, University of Potsdam, Nuthetal, Germany (MBS)

1 Stefan N, Schulze MB. Metabolic health and cardiometabolic risk clusters: implications for prediction, prevention, and treatment. *Lancet Diabetes Endocrinol* 2023; **11:** 426–40.
2 Ahlqvist E, Storm P, Käräjämäki A, et al. Novel subgroups of adult-onset diabetes and their association with outcomes: a data-driven cluster analysis of six variables. *Lancet Diabetes Endocrinol* 2018; **6:** 361–69.
3 Christensen DH, Nicolaisen SK, Ahlqvist E, et al. Type 2 diabetes classification: a data-driven cluster study of the Danish Centre for Strategic Research in Type 2 Diabetes (DD2) cohort. *BMJ Open Diabetes Res Care* 2022; **10:** e002731.
4 Dennis JM, Shields BM, Henley WE, Jones AG, Hattersley AT. Disease progression and treatment response in data-driven subgroups of type 2 diabetes compared with models based on simple clinical features: an analysis using clinical trial data. *Lancet Diabetes Endocrinol* 2019; **7:** 442–51.
5 Zou X, Zhou X, Zhu Z, Ji L. Novel subgroups of patients with adult-onset diabetes in Chinese and US populations. *Lancet Diabetes Endocrinol* 2019; **7:** 9–11.
6 Ke C, Narayan KMV, Chan JCN, Jha P, Shah BR. Pathophysiology, phenotypes, and management of type 2 diabetes mellitus in Indian and Chinese populations. *Nat Rev Endocrinol* 2022; **18:** 413–32.
7 Varghese JS, Narayan KMV. Ethnic differences between Asians and non-Asians in clustering-based phenotype classification of adult-onset diabetes mellitus: a systematic narrative review. *Prim Care Diabetes* 2022; **16:** 853–56.
8 Stefan N, Cusi K. A global view of the interplay between non-alcoholic fatty liver disease and diabetes. *Lancet Diabetes Endocrinol* 2022; **10:** 284–96.
9 Stefan N, Schick F, Birkenfeld AL, Häring HU, White MF. The role of hepatokines in NAFLD. *Cell Metab* 2023; **35:** 236–52.

Tuning of cellular insulin release by music for real-time diabetes control

Music consists of acoustic waves that are converted by the bony ossicles in the middle ear into mechanical vibrations. These vibrations activate mechanosensitive ion channels in hair cells,[1] causing membrane depolarisation and release of neurotransmitters, thereby influencing human emotion. Similar mechanosensitive ion channels are ubiquitous across all kingdoms of life. Examples include transient receptor potential channels,[2] piezo-type mechanosensitive ion channels (eg, Piezo1 and Piezo2),[3] bacterial small conductance mechanosensitive channels (MscS), and large conductance mechanosensitive channels (MscL).[4] Among them, modified *Escherichia coli* MscL has been expressed in mammalian cells to enable tension-controlled loading and trigger-inducible release of model cargoes.[5]

Many gene switches have been developed for use in next-generation cell-based therapies to treat multiple diseases.[6] However, systemic delivery of small-molecular trigger compounds faces pharmacokinetic challenges and can cause side-effects, and traceless triggers, such as light, ultrasound, magnetic fields, radio waves, electricity, and heat, also face various challenges. Thus, there is still a need for new switching modalities.

Here, we describe a music-inducible cellular control (MUSIC) system that functionally links music-actuated mechano-transduction by ectopically expressed MscL to calcium-triggered vesicular secretion, enabling engineered human cells to release stored insulin within minutes.

The design of our MUSIC cellular device involves rewiring the intracellular calcium surge actuated by calcium-permeable mechanosensitive channels in response to music to drive immediate calcium-triggered vesicular release of biopharmaceuticals (figure A). We generated stable transgenic clonal MUSIC-controlled insulin-releasing cell lines constitutively expressing mammalian Piezo1 or bacterial MscS or MscL, together with a pro-insulin expression unit in glucose-insensitive human pancreatic β cells. The cells were cultivated in standard 6-well plates with a flexible rubber bottom, placed on a customised box containing off-the-shelf loudspeakers (appendix pp 5–6). A sound level of 60 dB at 50 Hz, which is within the safe range for the human ear, effectively activated the channels (appendix p 5). MscL-transgenic cells ($MUSIC_{INS}$) showed the highest maximum and fold induction of insulin release combined with the lowest basal expression (appendix p 5). Note that cells in single-cell suspension cultures were insensitive to sound stimulation since they escaped sound-based mechanical stimulation by rotation when freely floating in the culture medium. Therefore, music-responsive cells need to be immobilised on the surface of the cell-culture dish in order respond to music (appendix p 7). The mechanistic connection between sound stimulation and insulin release by $MUSIC_{INS}$ is likely to be mediated by calcium. Indeed, imaging of MscL-positive and MscL-negative cells expressing the fluorescent calcium indicator GCaMP6s[7] showed significantly higher intracellular calcium levels in the former cell population after both had been sound-stimulated

See Online for appendix

(appendix pp 7, 21). Furthermore, sound-stimulated MUSIC$_{INS}$ cells showed increased insulin release when incubated in higher calcium chloride concentrations (appendix p 8). Finally, mechanical stimulation by piston-induced shear forces[8] also triggered significantly higher insulin secretion by MUSIC$_{INS}$ cells (appendix p 8). Taken together, these results support the idea that the sound waves act as mechanical forces to open the MscL channels and initiate calcium influx (appendix pp 7–8, 21).

To identify the optimum frequency range, we profiled vesicular insulin release by MUSIC$_{INS}$ cells within 15 min at a loudspeaker membrane acceleration of 50 m/s² (55–85 dB) for the bass and lower midrange (50–250 Hz) and below 25 m/s² (85 dB) for the midrange and treble (0·5–20 kHz) (appendix p 9). MUSIC$_{INS}$-mediated insulin release was greatest at 50–100 Hz,

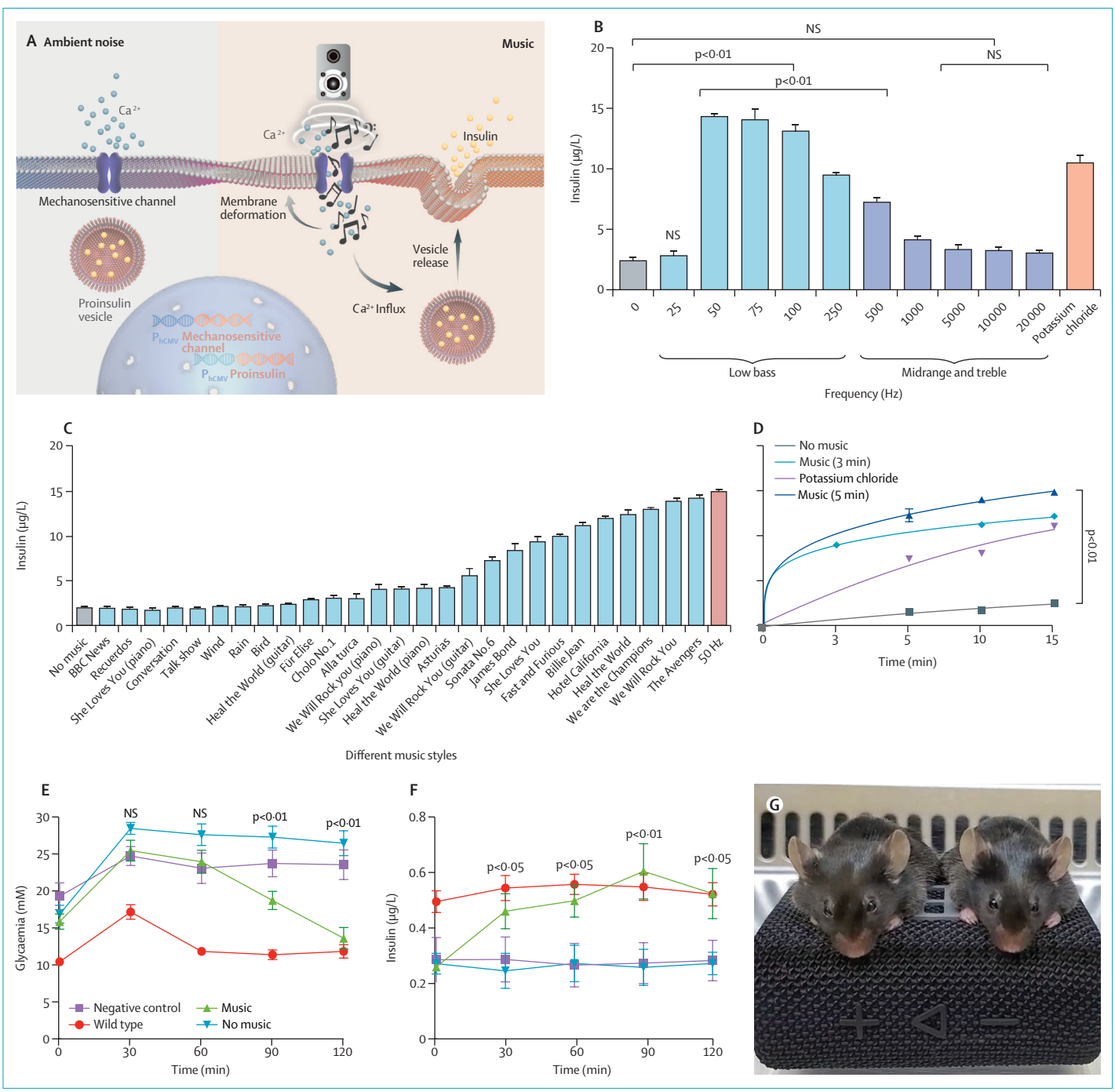

exceeding the response to potassium chloride, the gold-standard positive chemical depolarisation control (figure B). $MUSIC_{INS}$ cells showed maximum viability while providing the highest insulin release at 50 Hz and 50 m/s² (60 dB; appendix p 10).

Next, we acoustically stimulated $MUSIC_{INS}$ at 50 Hz and 60 dB for 15 min with a 5 s ON and 2 s OFF cycle, gradually increasing the OFF period to 120 s. Insulin release decreased with increasing OFF interval (appendix p 10). MUSIC activation requires at least 3 s of continuous music, which might protect the cellular device from inadvertent activation during everyday activities (appendix p 10).

We then validated $MUSIC_{INS}$'s insulin-release performance to different musical genres (figure C, appendix pp 11–12) at 85 dB, the average sound level when listening to music and quieter than a typical live concert (105–110 dB). Low-bass heavy popular music and movie soundtracks induced maximum insulin release, whereas responses to classical music and guitar music was more diverse and composition-specific. Environmental noises and speech did not trigger insulin release (appendix p 12).

We next analysed the dynamics of music-triggered insulin release. Queen's song, We Will Rock You, released almost 70% of insulin within 5 min, and release was complete within 15 min, similar to the dynamics of glucose-triggered insulin release by human pancreatic islets[9] (figure D).

Further, by exposing insulin-depleted $MUSIC_{INS}$ cells to a second music session after different intervals, we found that the cells reached a full insulin refill within 4 h consistently over several days (appendix p 13). This would be appropriate to attenuate glycaemic excursions associated with typical dietary habits.

For mouse experiments, we built a box containing two off-the-shelf loudspeakers that focus the acoustic waves via deflectors onto the belly of the animals (appendix pp 14–16, 21). $MUSIC_{INS}$ cells were immobilised in coherent hydrogel microcontainers whose persistence, efficacy, and immuno-protection have been clinically validated for human islet transplantation, and we confirmed music-sensitive insulin release by the microencapsulated cells (appendix p 17).

Type 1 diabetic C57BL/6J mice intraperitoneally implanted with microencapsulated $MUSIC_{INS}$ cells and exposed to low-bass acoustic waves at 60 dB (50 m/s²) for 15 min reached near wild-type blood insulin levels (appendix pp 14, 21). Queen's song *We Will Rock You* generated sufficient insulin to rapidly attenuate postprandial glycaemic excursions during glucose tolerance tests, whereas animals without implants or with implants but without music immersion remained severely hyperglycaemic (figure E; appendix p 21). Blood-insulin levels of music-immersed animals rose within minutes, reached wild-type levels, and peaked within 90 min (figure F). One 15 min per day music session restored wild-type blood insulin levels and reinstated normoglycemia (appendix p 14). Commercial headphones or ear plugs, such as Apple AirPods, did not trigger $MUSIC_{INS}$ (appendix pp 17, 21). $MUSIC_{INS}$ cells are triggered only if the sound waves directly impinge on the skin just above the implantation site for at least 15 min (appendix p 18). Various loud environmental noises, such as low flying aircrafts, lawn mowers, fire trucks, and horns, did not result in undesired insulin secretion when perceived from different distances and directions (appendix pp 18, 22).

With cell-based therapies beginning to provide opportunities for novel precision treatments, the Paracelsus paradigm that the dose makes the drug is shifting from pill-based administration of small-molecular drugs towards dynamic, gene-switch-controlled therapeutic gene expression and in-situ biopharmaceutical production.[6] Considering the limitations of existing gene switch triggers, we designed a music-responsive synthetic gene switch by rewiring music-based intracellular calcium influx by mechanosensitive channels to vesicular release of protein therapeutics. Several methods exist to sensitise cells to membrane deformation, which might be evoked by atomic force microscopy, blunt probes, pipette pressure, and shear flow, but none is sufficiently sensitive to capture typical audio

Figure: **Design and characterisation of the $MUSIC_{INS}$ cells**

(A) Sound waves induce membrane deformation of engineered β cells constitutively expressing a mechanosensitive channel and a synthetic proinsulin construct, triggering intracellular Ca^{2+} increase due to opening of the mechanosensitive channel, which initiates the release of insulin from the secretory vesicles. (B) Insulin release by $MUSIC_{INS}$ cells stimulated during 15 min at the indicated frequencies (6 [8%] of 72). The statistical significance of the differences between the 0 Hz group, and the low bass and midrange and treble groups, was calculated. $MUSIC_{INS}$ cells stimulated with 40 mM potassium chloride were used as a positive control. (C) In-vitro characterisation of insulin secretion levels after exposure of $MUSIC_{INS}$ cells to different music styles (6 [3%] of 174). (D) Music-stimulated insulin secretion kinetics. $MUSIC_{INS}$ cells were stimulated with music for 3 and 5 min by the speaker setup. $MUSIC_{INS}$ cells without music stimulation or treated with potassium chloride (40 mM) were used as negative control and positive controls, respectively (6 [25%] of 24). The statistical significance of the differences between the no music and music (5 min) groups was analysed. (E) Glucose tolerance test. Wild-type or type 1 diabetic C57BL/6J mice were intraperitoneally implanted with $MUSIC_{INS}$. The mice were exposed to music for 15 min after intraperitoneal injection of 1·5 g of glucose per kg bodyweight (8 [25%] of 32). The statistical significance of the differences between the negative control and music groups was analysed at the various timepoints. (F) Time course of blood insulin levels. Wild-type or type 1 diabetic mice implanted intraperitoneally with alginate-based hollow microcontainers were fasted for 4 h before music stimulation for 15 min (8 [25%] of 32). The statistical significance of the differences between the negative control and the music groups was analysed at the various timepoints. Blood samples were collected at the indicated timepoints. Non-stimulated mice were used as controls. The statistical significance of the difference between the 50 Hz and music stimulation group and the no 50 Hz and music stimulation group was calculated. Data are mean (SEM). (G) Type 1 diabetic mice exposed to music treatment by portable music. Statistical analysis was done with a two-tailed Mann-Whitney non-parametric test. NS=not significant. MUSIC= music-inducible cellular control. P_{hCMV}=human cytomegalovirus immediate early promoter.

frequencies. We showed that MscL opens in response to increased plasma membrane tension following audible acoustic stimulation, and the resulting calcium ion influx can drive vesicular release of a protein pharmaceutical. Specifically, MUSIC triggers insulin release in response to compositions containing low-bass frequency patterns. Therapeutic MUSIC sessions would still be compatible with listening to other types of music, or listening to all types of music via headphones.

Compared with classical transcription-based transgene-control modalities,[6] MUSIC's vesicular secretion is much faster, and also enables a discontinuous peak delivery of protein therapeutics that is especially appropriate for metabolic interventions, and is compatible with standard drug administration schemes.[6] With only 4 h required for a full refill, MUSIC can provide several therapeutic doses a day. This would match the typical needs of people with type 2 diabetes consuming three meals a day, and for whom administration of prandial insulin is an established treatment option, as they do not have capability for early postprandial insulin secretion from preformed insulin.[10] In addition, the time needed to fully refill the secretory granular offers a safety feature against the risk of hypoglycaemia, once the appropriate dose is established.

MUSIC-transgenic cells can be stimulated by portable battery-powered commercial loudspeakers, with their bellies facing the speaker (figure G; appendix p 22), making multiple daily dosing of biopharmaceuticals straightforward in the absence of medical infrastructure or staff, simply by having the patient listen to the prescribed music. To illustrate MUSIC's translational potential, we showed that MUSIC-driven insulin release stimulated by off-the-shelf loudspeakers attenuated postprandial glycaemic excursions and restored normoglycaemia in a mouse model of type 1 diabetes. This finding, combined with the safety feature offered by the refill period, suggests that therapeutic cell implants exposed to specific music and releasing crucial biopharmaceuticals in response could be an interesting option for cell-based therapies, especially where the need for frequent dosing raises compliance issues.

We declare no competing interests. This work was supported by a European Research Council advanced grant (ElectroGene, grant number 785800) and in part by the Swiss National Science Foundation NCCR Molecular Systems Engineering. HZ acknowledges the support by the Chinese Scholarship Council (201806780020). We thank Paul Argast, Nik Franko, Tobias Strittmatter, and Henryk Zulewski for their generous advice, Tobias Strittmatter and Jinbo Huang for sharing plasmids before publication, and Hans-Michael Kaltenbach for advice on statistics.

*Haijie Zhao, Shuai Xue, Marie-Didiée Hussherr, Peter Buchmann, Ana Palma Teixeira, *Martin Fussenegger*
fussenegger@bsse.ethz.ch

Department of Biosystems Science and Engineering, ETH Zurich, CH-4058 Basel, Switzerland (HZ, SX, M-DH, PB, APT, MF); Faculty of Science, University of Basel, Switzerland (MF)

1 Pan B, Akyuz N, Liu XP, et al. TMC1 forms the pore of mechanosensory transduction channels in vertebrate inner ear hair cells. *Neuron* 2018; **99:** 736–53.e6.
2 Duque M, Lee-Kubli CA, Tufail Y, et al. Sonogenetic control of mammalian cells using exogenous Transient Receptor Potential A1 channels. *Nat Commun* 2022; **13:** 600.
3 Coste B, Mathur J, Schmidt M, et al. Piezo1 and Piezo2 are essential components of distinct mechanically activated cation channels. *Science* 2010; **330:** 55–60.
4 Sukharev SI, Blount P, Martinac B, Blattner FR, Kung C. A large-conductance mechanosensitive channel in E. coli encoded by mscL alone. *Nature* 1994; **368:** 265–68.
5 Doerner JF, Febvay S, Clapham DE. Controlled delivery of bioactive molecules into live cells using the bacterial mechanosensitive channel MscL. *Nat Commun* 2012; **3:** 990.
6 Krawczyk K, Xue S, Buchmann P, et al. Electrogenetic cellular insulin release for real-time glycemic control in type 1 diabetic mice. *Science* 2020; **368:** 993–1001.
7 Chen TW, Wardill TJ, Sun Y, et al. Ultrasensitive fluorescent proteins for imaging neuronal activity. *Nature* 2013; **499:** 295–300.
8 Strittmatter T, Argast P, Buchman P, Krawczyk K, Fussenegger M. Control of gene expression in engineered mammalian cells with a programmable shear-stress inducer. *Biotechnol Bioeng* 2021; **118:** 4751–59.
9 Nesher R, Cerasi E. Modeling phasic insulin release: immediate and time-dependent effects of glucose. *Diabetes* 2002; **51** (suppl 1)**:** S53–59.
10 Bretzel RG, Nuber U, Landgraf W, Owens DR, Bradley C, Linn T. Once-daily basal insulin glargine versus thrice-daily prandial insulin lispro in people with type 2 diabetes on oral hypoglycaemic agents (APOLLO): an open randomised controlled trial. *Lancet* 2008; **371:** 1073–84.

THE LANCET
Diabetes & Endocrinology

Supplementary appendix

This appendix formed part of the original submission. We post it as supplied by the authors.

Supplement to: Zhao H, Xue S, Hussherr M-D, Buchmann P, Teixeira AP, Fussenegger M. Tuning of cellular insulin release by music for real-time diabetes control. *Lancet Diabetes Endocrinol* 2023; **11:** 637–40.

Supplementary appendix

Tuning of cellular insulin release by music for real-time diabetes control

Haijie Zhao[1], Shuai Xue[1], Marie-Didiée Hussherr[1], Peter Buchmann, Ana Palma Teixeira[1], Martin Fussenegger[1,2,*]

[1]Department of Biosystems Science and Engineering, ETH Zurich, Mattenstrasse 26, CH-4058 Basel, Switzerland.

[2]Faculty of Science, University of Basel, Mattenstrasse 26, CH-4058 Basel, Switzerland

[*]Corresponding author. E-mail: fussenegger@bsse.ethz.ch

Supplementary appendix: Tuning of cellular insulin release by music for real-time diabetes control.

Supplementary Appendix – Table of contents:

Page:

Material and Methods

Cell culture and transfection. Human pancreatic 1.1E7 cells (cat. no. 10070101-1VL, Sigma-Aldrich) were cultured in Roswell Park Memorial Institute 1640 medium (RPMI, cat. no. 72400-021, Thermo Fischer Scientific) supplemented with 10 % foetal bovine serum (FBS, cat. no. F7524, lot no. 022M3395, Sigma-Aldrich), 100 U/mL penicillin and 100 µg/mL 100x penicillin-streptomycin solution (cat. no. L0022, Biowest). Cells were cultivated at 37 ˚C in a humidified atmosphere containing 5% CO_2. For passaging, cells were detached by incubation for 3 min at 37 °C in 0.05% trypsin-EDTA (cat. no. 25300-054, Life Technologies), collected by centrifugation for 1 min at 200 x g and resuspended in FBS-containing RPMI at 1.5 x 10^5 cells/mL. Cell densities were quantified using an automated cell counter (CellDrop™, DeNOVIX). For transfection, the cells were seeded at a density of 3.5 x 10^5 per cm^2 and cultivated for 24 h before adding a lipofectamine (Lipofectamine™ 3000, Thermo Fisher Scientific) transfection mixture containing a total of 0.5 µg of plasmid DNA per cm^2 of transfected cells for another 24 h.

Establishment of stable MUSIC$_{INS}$ cells. Human pancreatic 1.1E7 cells (2 x 10^6 cells/mL) were co-transfected as described above with (i) pLX304[109] (P_{hCMV}-Proinsulin-NanoLuc-pA, 4.5 µg), encoding constitutive expression of insulin and nanoluciferase, (ii) pHZ10 (ITR-P_{hCMV}-MscL-P2A-PuroR-pA:P_{RPBSA}-BFP-P2A-Zeo-pA-ITR; 5.5 µg) encoding, besides the reporter gene (BFP) and selection markers (PuroR, Zeo), the constitutive expression of the *Escherichia coli* large-conductance mechanosensitive channel (MscL), and (iii) 0.5 µg of pCMV-T7-SB100[111] (P_{hCMV}-SB100X-pA) containing the constitutive expression unit for the Sleeping Beauty transposase SB100X. The cells were cultivated for clonal selection in culture medium containing 25 µg/mL of puromycin (cat. no. A1113803, Thermo Fisher Scientific) or 25 µg/mL of zeocin (cat. no. R25005, Thermo Fisher Scientific). For isogenic cell lines expressing the mammalian mechanosensitive receptor PIEZO1 or the prokaryotic small-conductance mechanosensitive channel MscS, pHZ10 was replaced by pTS391 (ITR-P_{hCMV}-PIEZO1-pA:P_{RPBSA}-mRubby-P2A-PuroR-pA-ITR) or pTS414 (ITR-P_{hCMV}-MscS-pA:P_{RPBSA}-BFP-P2A-Zeo-pA-ITR), respectively. For the assembly of β-cell organoids, MUSIC$_{INS}$ were detached as described above, washed twice in RPMI medium, and 5 x 10^5 cells/mL were seeded in 24-well ultra-low attachment plates (cat. no. CLS3473-24EA, Corning Inc.) for 12 hours. The spontaneously assembled MUSIC$_{INS}$ microtissues were collected by centrifugation for 5 min at 200 x g and used in stimulation experiments.

Analytical assays. Cell viability. Cell viability was quantified by incubating the cells for 2 hours with resazurin (50 µg/mL, cat. no. R7017, Sigma-Aldrich) before recording the fluorescence at 540/590 nm (Tecan Infinite 200 PRO plate reader, Tecan Group AG) [112]. **NanoLuc luciferase.** NanoLuc luciferase was quantified in cell culture supernatants using the Nano-Glo® Luciferase Assay System (cat. no. N1110, Promega). In brief, 10 µL of cell culture supernatant was added per well of a black 384-well plate and mixed with 10 µL of substrate-containing assay buffer. Total luminescence was quantified at 460/20 nm (Tecan GENios PRO plate reader, Tecan Group AG). **Insulin.** Insulin was quantified by an ELISA kit (cat. no. 10-1247-01, Mercordia). **Glucose.** Blood-glucose levels were quantified using the clinically licensed Contour®Next test strips and Contour®Next ONE reader[113] (Ascensia Diabetes Care).

Music stimulation. Cell culture. Engineered cells were cultivated in flexible-bottomed 6-well BioFlex® culture plates (cat. no. BF-3001C, Flexcell) at a density of 3.5 x 10^5 cells/cm^2 for 48 h before the plate was fixed onto a customised speaker set-up that directly exposes the monolayer cultures to the soundwaves generated by the speaker (cat. no. W3-1750S, TB-Speakers). The customised speaker set-up contains six holes matching the size of the individual wells of a 6-well plate base, thereby locating the flexible rubber membrane of the BioFlex® culture plate above the loudspeaker. To maintain the pressure balance inside the device, an additional hole was made in the side of the loudspeaker device. The frequency was set by a pulse generator (JT-JDS6600-LITE, JOYIT) and the output intensity was controlled by a 2 x 50 W stereo amplifier (T21, Renkforce). Speaker acceleration was monitored by an accelerometer (ADXL326, Adafruit Industries) and an oscilloscope (DS1052E, Rigol Technologies). The sound level (dB) was measured with a sound level meter (SL-10, Voltcraft). To set the exposure times and intervals, the speaker system was programmed using a software-controlled switchboard (cat. no. MEGA 2560, Arduino, software version 1.8.11, Arduino). **Mice.** The speaker box for music stimulation of mice implanted with microencapsulated $MUSIC_{INS}$ cells (see **Fig. S10** and **Fig. S11**) was handmade with polyvinyl chloride (PVC) by an external workshop (G+B PLEX AG, Switzerland), and contains two speakers (cat. no. W3-1750S, TB-Speakers), a centering base, a deflector shelf, a tunnel lock and a tunnel gate. The animals were exposed to music for 15 min at 50 Hz and 60 dB.

Calcium imaging. Human embryonic kidney (HEK-293) cells were transfected with the genetically encoded calcium indicator GCaMP6s (P_{hCMV}-GCaMP6s-pA) in the presence or absence of constitutive expression of the MscL channel (P_{hCMV}-MscL-pA). A 3D-printed customized adapter for a 6-well BioFlex® culture plate was used in a Nikon Eclipse Ti2-E wide-field microscope (Nikon Instruments Europe B.V.). Before music stimulation, the cell

culture medium was replaced by phenol red-free DMEM (cat. no. 21063029, Thermo Fisher Scientific). During music stimulation, the speaker is buckled upside down on the 6-well plate. Images were collected via a 10x objective lens with 100 ms exposure time and 1 s duration.

Microencapsulation and implantation of $MUSIC_{INS}$ cells. To protect the human $MUSIC_{INS}$ cells from the mouse immune system while enabling free diffusion of nutrients and therapeutic proteins such as insulin, we used clinical trial-validated, FDA-licensed alginate-based encapsulation technology[114]. $MUSIC_{INS}$ were microencapsulated into coherent alginate-poly(L-lysine) (PLL)-alginate microcapsules of 400 μm in diameter by mixing 7.5 x 10^7 $MUSIC_{INS}$ with 12 mL alginate (cat. no. 11061528; Büchi, Switzerland), 200 mL 0.05 % PLL solution (cat. no. PLKB50, Alamanda Polymers). The encapsulator (B-395 Pro, Büchi, Switzerland) was set to the following parameters: 200 μm nozzle with a vibration frequency of 1025 Hz, a 25 mL syringe operated at a flow rate of 20 mL/min and 1.1 kV voltage for bead dispersion. Then 5 x 10^6 microencapsulated cells in 0.5 mL of serum-free DMEM (500 cells/capsule) were intraperitoneally (i.p.) implanted through a standard 5 mL syringe equipped with a 21-gauge needle.

Animal experimentation. Type-1 diabetic mice were established by fasting 8-week-old C57BL/6J mice (Janvier Labs) for 4 h per day for five consecutive days while injecting a single dose per day of freshly diluted streptozotocin (STZ, cat. no. S0130, Sigma-Aldrich; 50 mg/kg in 300 μL sodium citrate buffer adjusted to pH 4.3). Type-1 diabetes-associated persistent fasting hyperglycemia was confirmed after six days by blood-glucose profiling. Fasting glycemia was measured after 8 h. For glucose-tolerance tests, treated animals were intraperitoneally injected with 1.5 g/kg glucose and blood glucose levels were recorded at regular intervals. Insulin was quantified in blood serum collected using Microtainer® serum separator tubes (cat. no. 365967, Becton Dickinson). All animal experiments were approved by the authorities of the Canton of Basel-Stadt, Switzerland (license number: 2996/30779) and conducted by Shuai Xue and Marie-Didiée Hussherr at the Department of Biosystems Science and Engineering (D-BSSE) of the ETH Zurich in Basel.

Statistical analysis. For the in vitro experiments, all the cell monolayers were derived from the same cell source, which was used across all replicates and conditions in order to reduce biological variation. Our unit of analysis is a monolayer of cells cultivated in a well of a standard 6-well cell culture plate. For each treatment group (no stimulation, different sound/music stimulation), we simultaneously performed at least 3 biological replicates consisting of cell monolayers seeded from the same cell batch. Each of these experiments was independently repeated three times using batches of cells with different passage numbers. For

the in vivo experiments, each animal represents an independent unit of analysis, and each treatment group consists of at least 5 mice. The relative fluorescence (indicative of the resazurin levels) is the dependent variable in the cell viability experiment. The glycemia level is the dependent variable in the GTT experiment. The concentration of insulin is the dependent variable in other experiments. Data are means ± SEM. Statistical analysis was done with a two-tailed Mann-Whitney non-parametric test (n = 6) as implemented in a commercially available software package (Prism 9, GraphPad Software, USA). Confidence interval (CI) = 95%. n.s. not significant, *P < 0.05, **P < 0.01, ***P < 0.001.

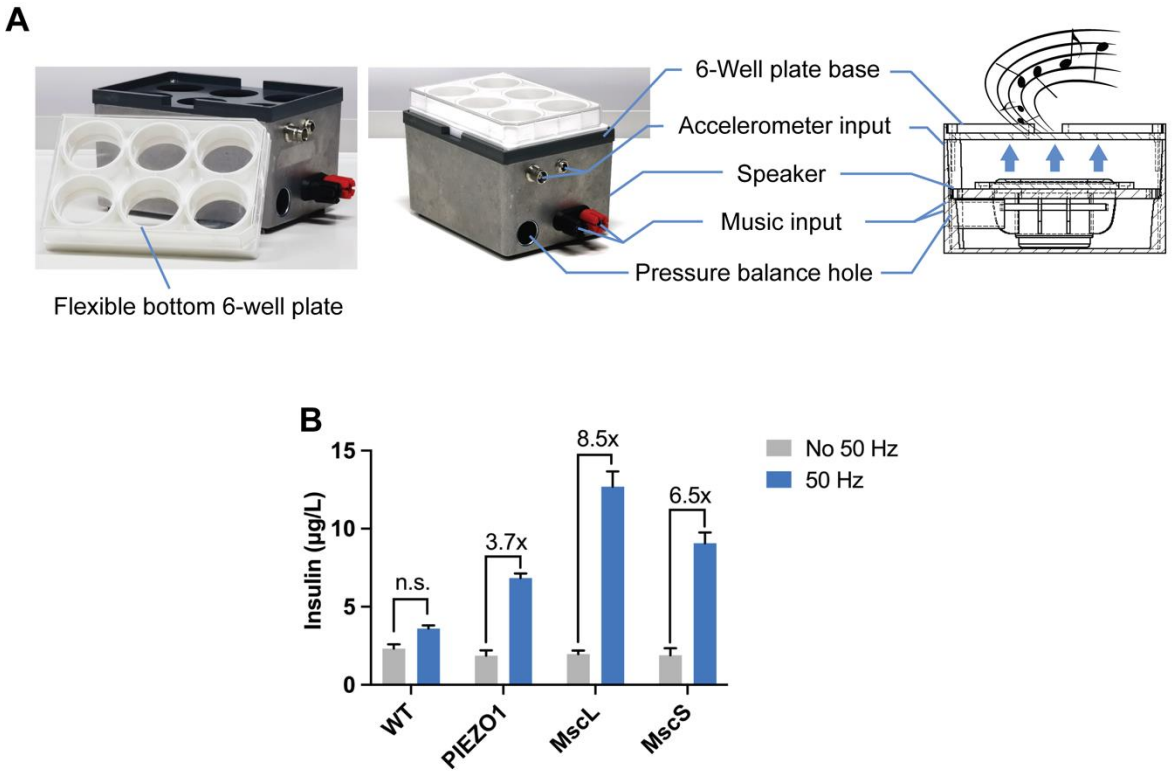

Figure S1. Design of the music-sensitive inducible cell system ($MUSIC_{INS}$ cells). (**A**) Image and illustration of the sound exposure device used for in vitro studies. The compact setup includes a speaker, pressure-balancing hole and 6-well plate base, which generates pressure on the flexible bottom 6-well plate. (**B**) Insulin secretion levels by engineered cells stably expressing three different MS channels, not exposed to sound or exposed to 50 Hz at 60 dB (50 m/s^2) during 15 min. Cells transfected with an empty plasmid were used as the control (n = 4).

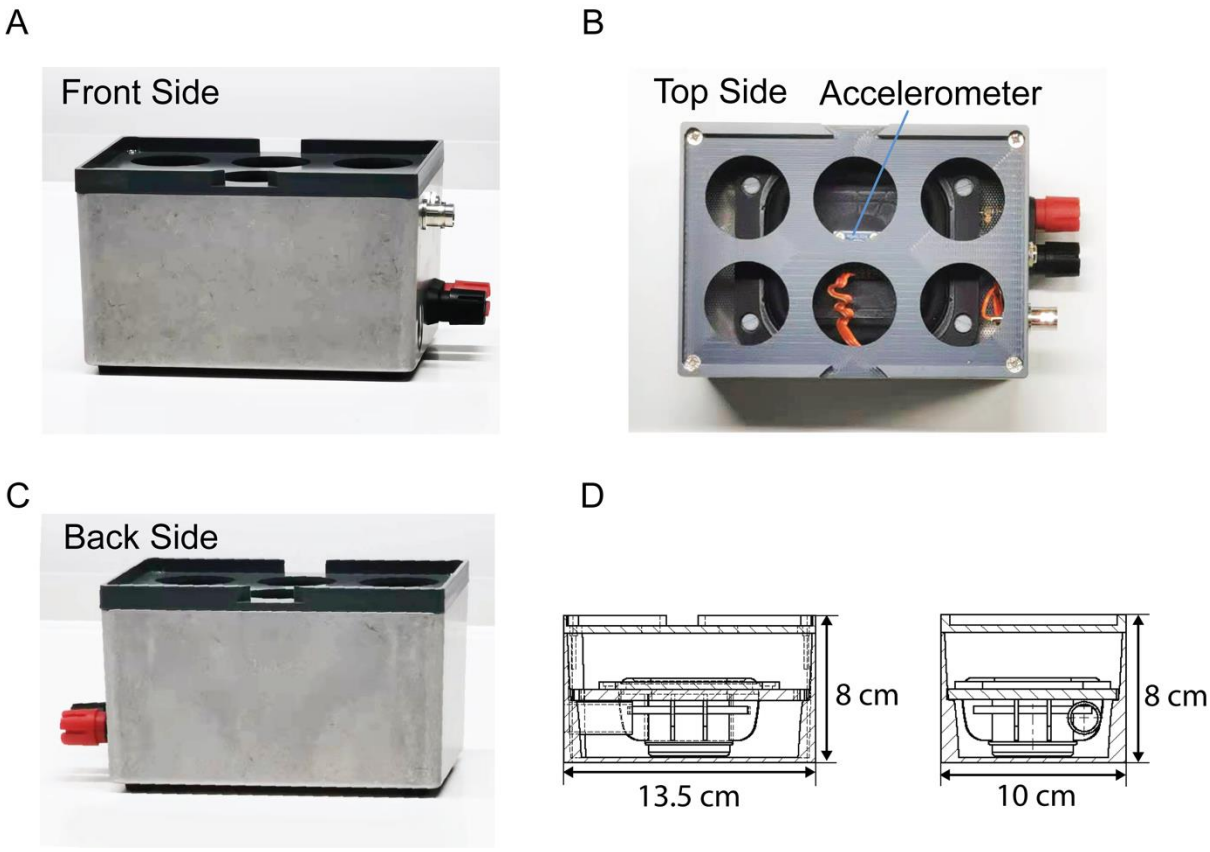

Fig. S2. (A - C) Three-dimensional and perspective views of the speaker system used for in vitro study, **(D)** with scale details.

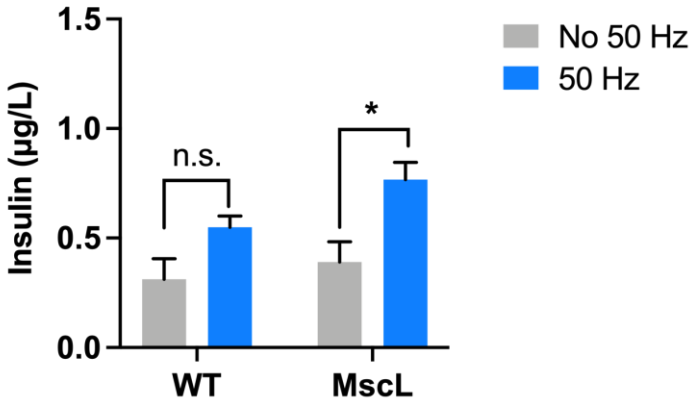

Figure S3. Stimulation of suspended β cell clusters from wild-type (WT) or MscL engineered mice. Aliquots of a suspension of β-cell clusters were transferred to a flexible-bottom 6-well plate and exposed to the speaker system (0.1 V, 50 Hz) for 15 min. Data are means ± SEM. Statistical analysis was done with a two-tailed Mann-Whitney non-parametric test (n = 6). n.s. not significant, *P < 0.05. The P value indicates the significance of differences between the "No 50 Hz" and "50 Hz" groups.

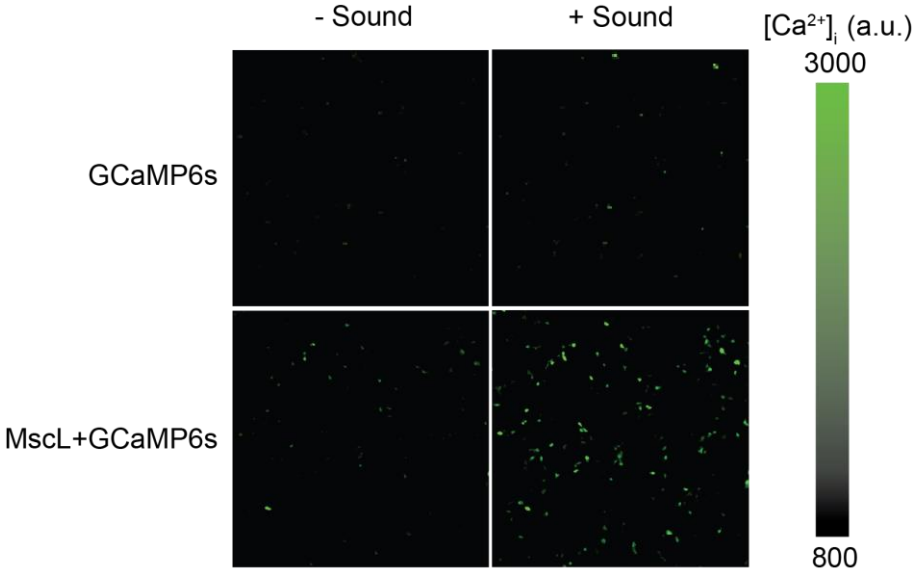

Figure S4. Intracellular calcium imaging. Representative quantitative intracellular calcium fluorescence micrographs of cells transiently transfected with MscL and/or the genetically encoded calcium sensor GCaMP6s and cultivated in the presence or absence of sound stimulation for 10 min at 70 Hz. a.u., arbitrary units. (See Movie S1 for sound-stimulated intracellular calcium dynamics).

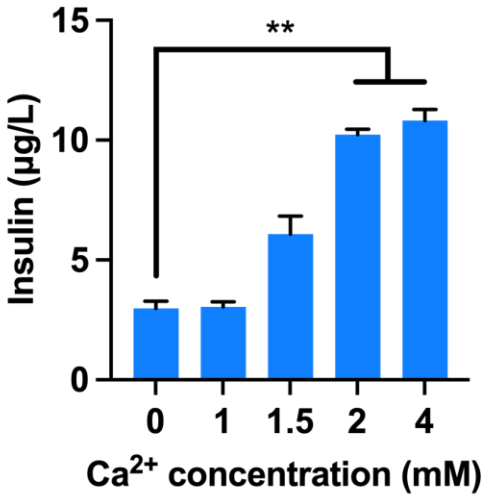

Figure S5. Insulin secretion by sound-stimulated $MUSIC_{INS}$ cells (50 Hz during 15 min) cultured in medium with different calcium chloride concentrations. Data are means ± SEM. Statistical analysis was done with a two-tailed Mann-Whitney non-parametric test (n = 6). **P < 0.01. The P value indicates the significance of differences between the "0 mM" group and "2 mM" or "4 mM" groups.

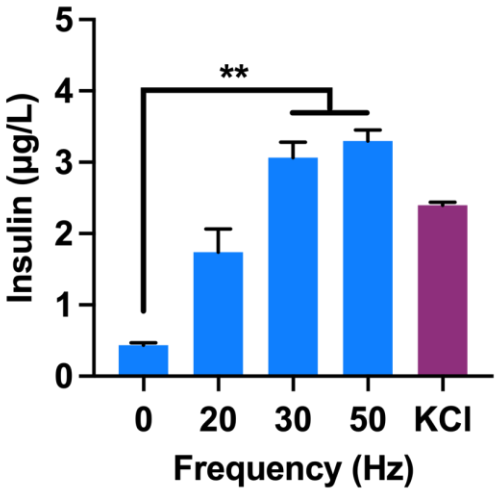

Figure S6. Insulin secretion by $MUSIC_{INS}$ cells stimulated with piston-induced shear forces at different frequencies. Data are means ± SEM. Statistical analysis was done with a two-tailed Mann-Whitney non-parametric test (n = 6). **P < 0.01. The P value indicates the significance of differences between the "0 Hz" group and "30 Hz" or "50 Hz" groups.

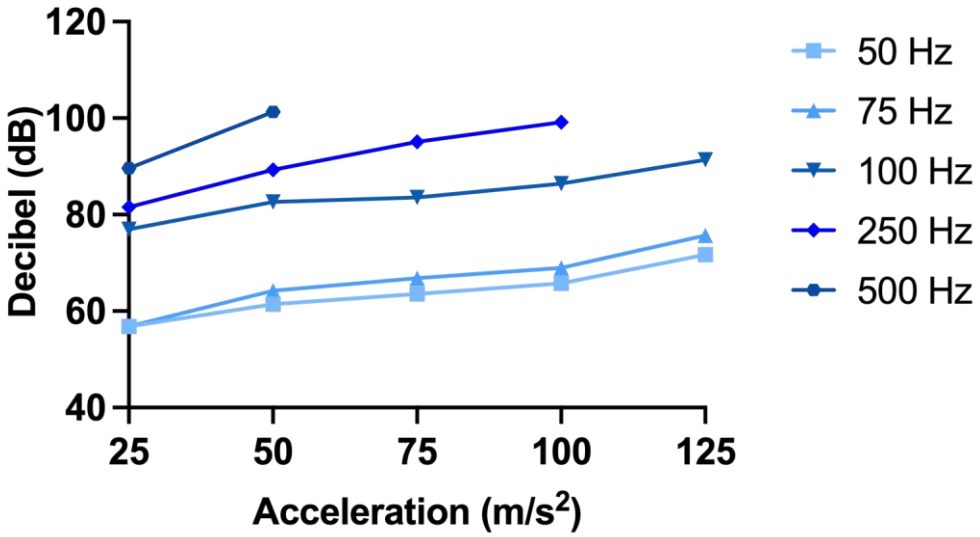

Figure S7. Correlation of sound intensity (decibel) and acceleration generated by the speaker setup in the frequency range from 50 to 500 Hz.

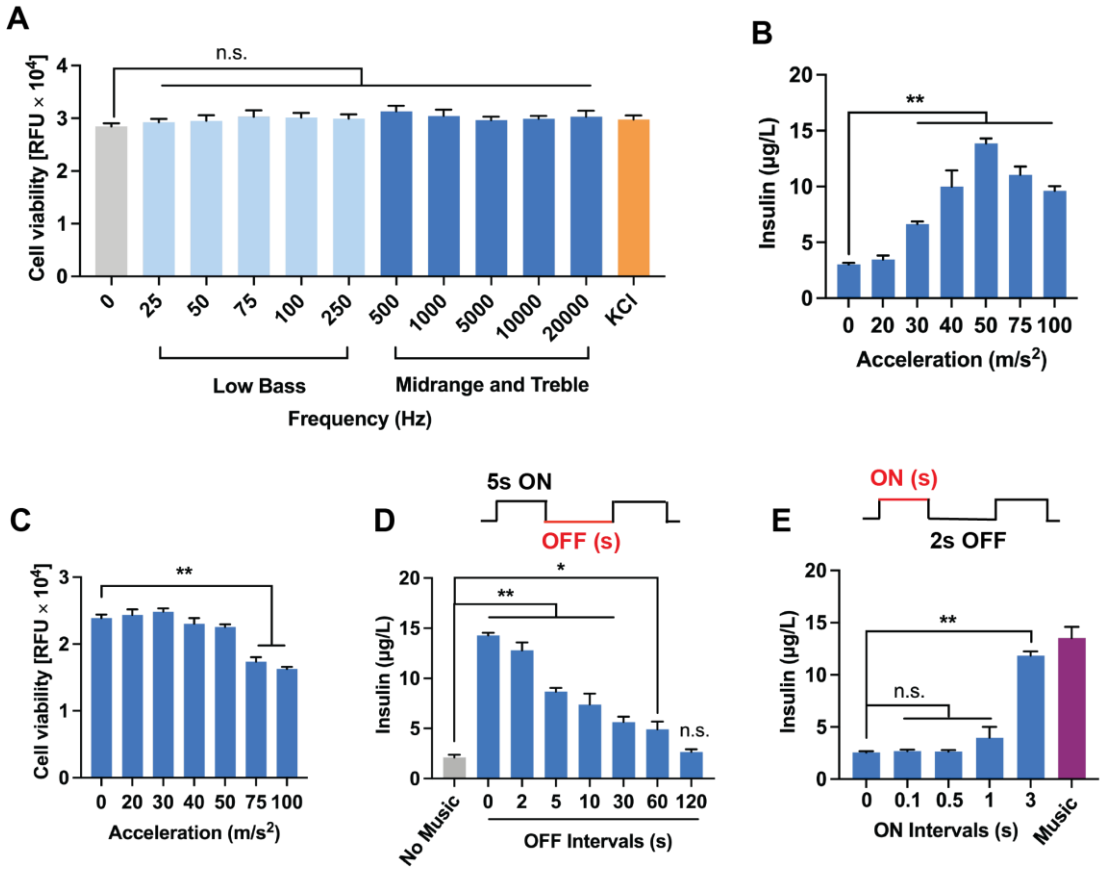

Figure S8. Characterization of the responses of $MUSIC_{INS}$ cells to different sound programs. (**A**) Cell viability was measured by resazurin assay after sound stimulation at the indicated frequencies (n = 6). Statistical analysis between "0 Hz" group and the "low bass" and "midrange and treble" groups is shown. (**B**) Voltage effect. Sound stimulation was performed at the indicated voltages for 15 min at 60 dB. (**C**) Cell viability was measured by resazurin assay after sound stimulation at the indicated voltages (n = 6). The statistical significance of the differences between the "0 m/s^2" group and the different acceleration groups was analysed. (**D**) Cells were stimulated at 60 dB (50 m/s^2) and 50 Hz for 15 min, using programmed sound patterns with 5 s on and the indicated time off (n = 6). The statistical significance of the differences between the "No music" group and the different "off intervals" groups was analysed. (**E**) Cells were stimulated at 60 dB (50 m/s^2) and 50 Hz for 15 min, programming sound patterns with 2 s off and the indicated time on (n = 6). The statistical significance of the differences between the "Music" and different "on intervals" groups was analysed. Data are means ± SEM. n.s. not significant, *P < 0.05, **P < 0.01. Two-tailed Mann-Whitney non-parametric tests were used for statistical analysis in all panels.

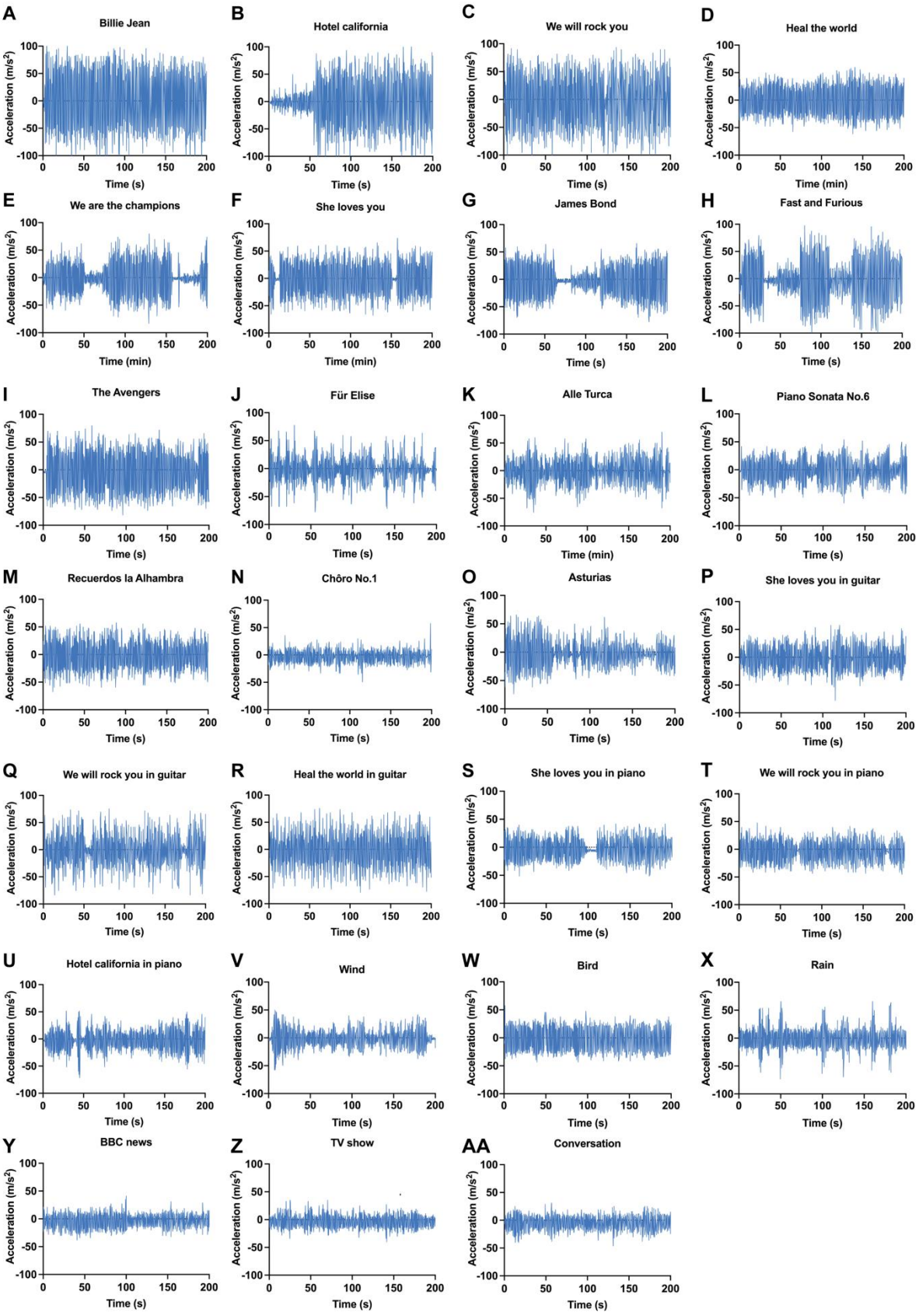

Figure S9. Recordings of acceleration pulses generated by different songs at 85 dB.

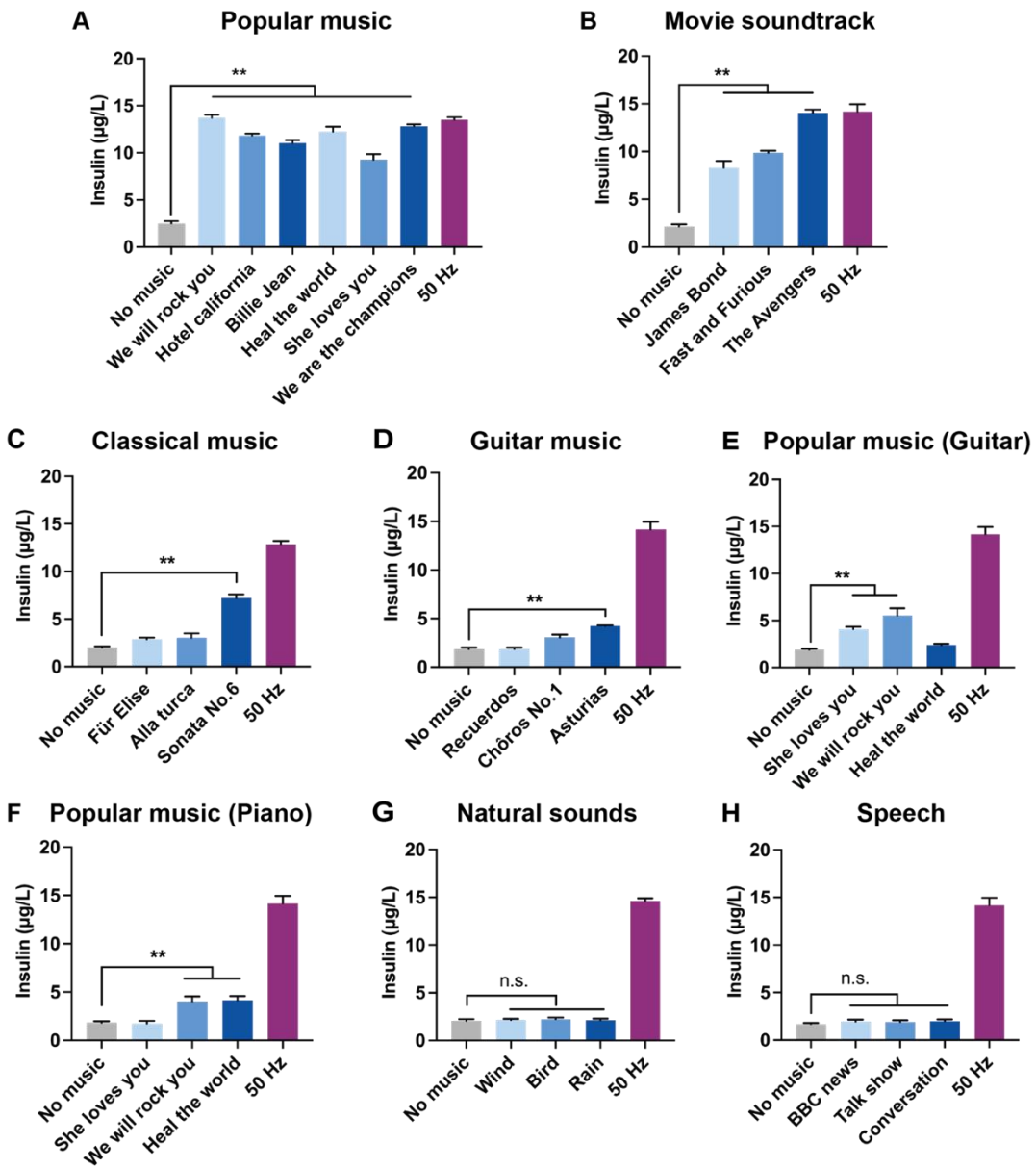

Figure S10. In vitro characterization of the responses of MUSIC$_{INS}$ cells to different songs. MUSIC$_{INS}$ cells were stimulated during 15 min with (**A**) Popular music, including "We Will Rock You", "Hotel California", "Billie Jean", "Heal the World", "She Loves You" and "We are the Champions", (**B**) Movie soundtracks, including James Bond ("James Bond Theme"), Fast and Furious ("See you again") and The Avengers ("Live to rise"), (**C**) Classical music, including Beethoven's "Für Elise", Mozart's "Alla Turca" and Beethoven's "Sonata No.6", (**D**) Guitar music, including Francisco Tárrega's "Recuerdos de la Alhambra", Heitor Villa-Lobos's " Chôros No.1", Isaac Albeniz's "Asturias", and popular music interpretations of original compositions on (**E**) guitar and (**F**) piano, (**G**) recorded naturals sounds such as wind, bird song and the sound of rain, (**H**) speech including "BBC news", "talk show" and "conversation". Stimulation with sound waves at 50 Hz was used as a positive control. Data

are means ± SEM. Statistical analysis was done with a two-tailed Mann-Whitney non-parametric test (n = 6). n.s. not significant, **P < 0.01. The P value indicates the significance of differences between the “No Music” group and the different types of music/sounds.

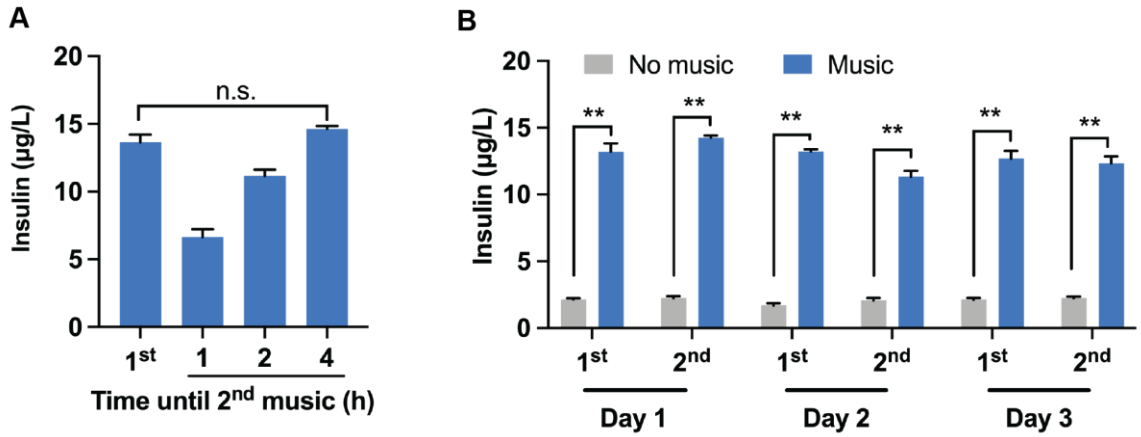

Figure S11. In vitro functionality of $MUSIC_{INS}$ cells. The track "We Will Rock You" was used for this study. (**A**) Reloading kinetics of vesicular insulin. Cells were stimulated twice for 15 min with the indicated time interval. The statistical significance of the differences between the “1st stimulation” group and the “4 h until 2nd music” group was analysed. (**B**) Reversibility assay. Electro-sensitive cells were stimulated twice daily for 15 min with a four-hour interval for a period of 3 days. The statistical significance of the differences between “No music” and “Music” groups was analysed. Data are means ± SEM. n.s. not significant, **P < 0.01. Two-tailed Mann-Whitney non-parametric tests were used for statistical analysis in both panels (n = 6).

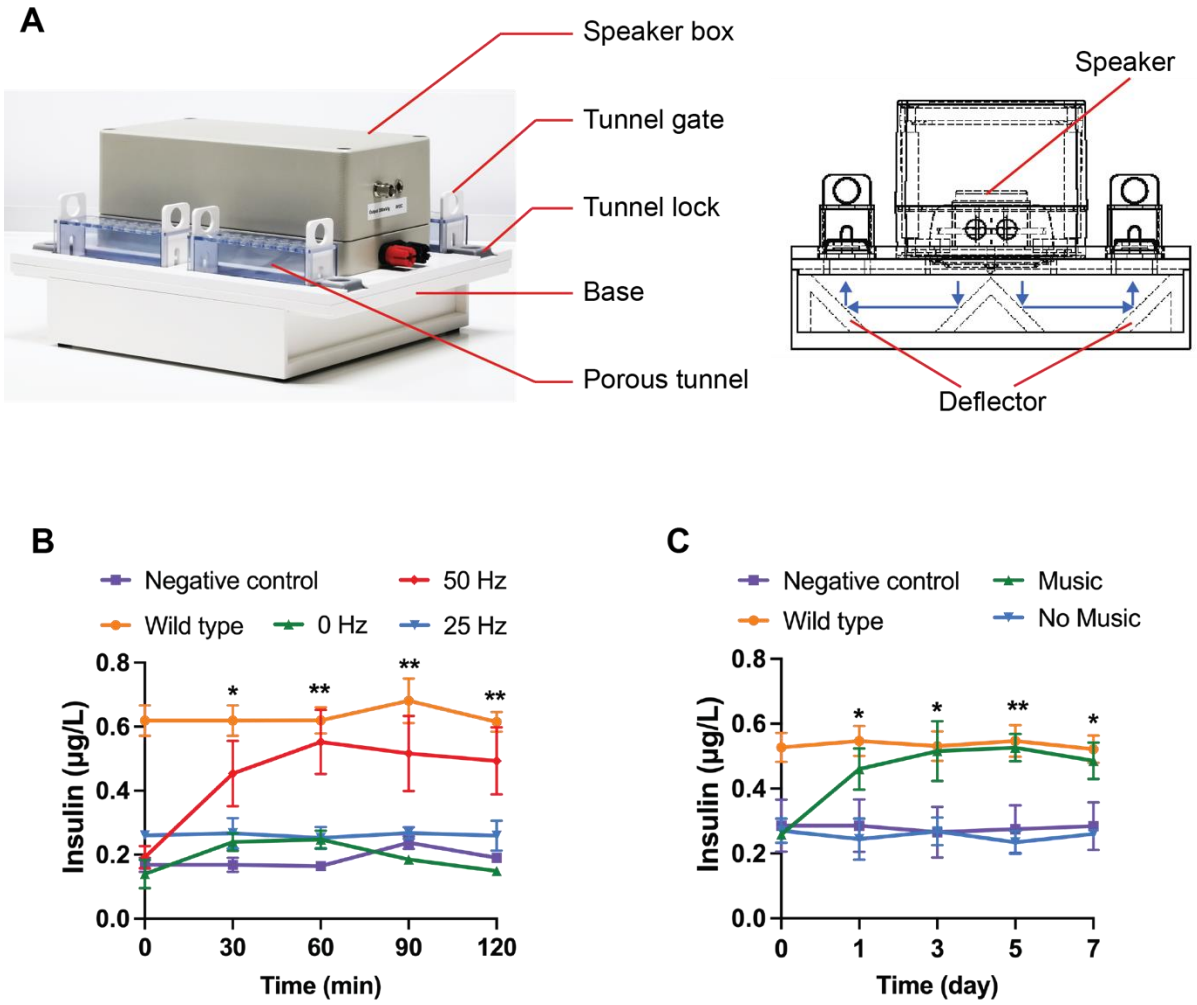

Figure S12. Design of the in vivo sound stimulation setup and in vivo characterization of $MUSIC_{INS}$ cells. **(A)** Picture **(left)** and illustration **(right)** of the speaker setup for the in vivo study. **(B)** Frequency. The type-1 diabetic mice were exposed to different frequencies at 50 m/s^2 for 15 min after intraperitoneally (i.p.) implantation of encapsulated $MUSIC_{INS}$ cells (n = 5). **(C)** The microcontainers were intraperitoneally implanted into type-1 diabetic mice and insulin levels were recorded every 2 days after 15 min of music stimulation, over a period of 7 days. Non-implanted type-1 diabetic mice were used as negative control. The statistical significance of the differences between the "Negative control" group and "Music" group was analysed using a two-tailed Mann-Whitney non-parametric test (n = 8). Data are means ± SEM. *P < 0.05, **P < 0.01.

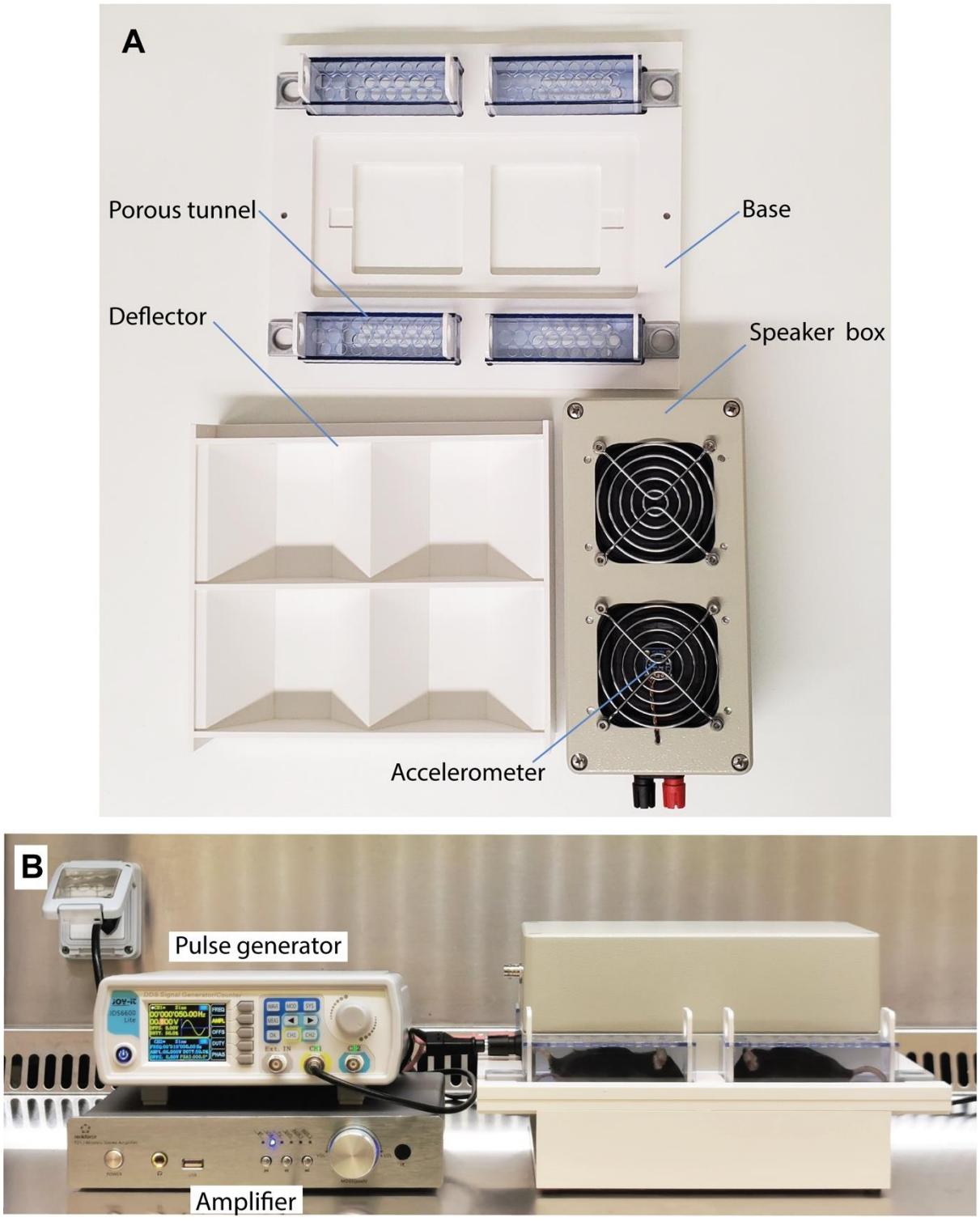

Figure S13. Photos of the speaker setup for the in vivo study. (A) The picture of the speaker setup components. (B) Speaker setup with amplifier and pulse generator.

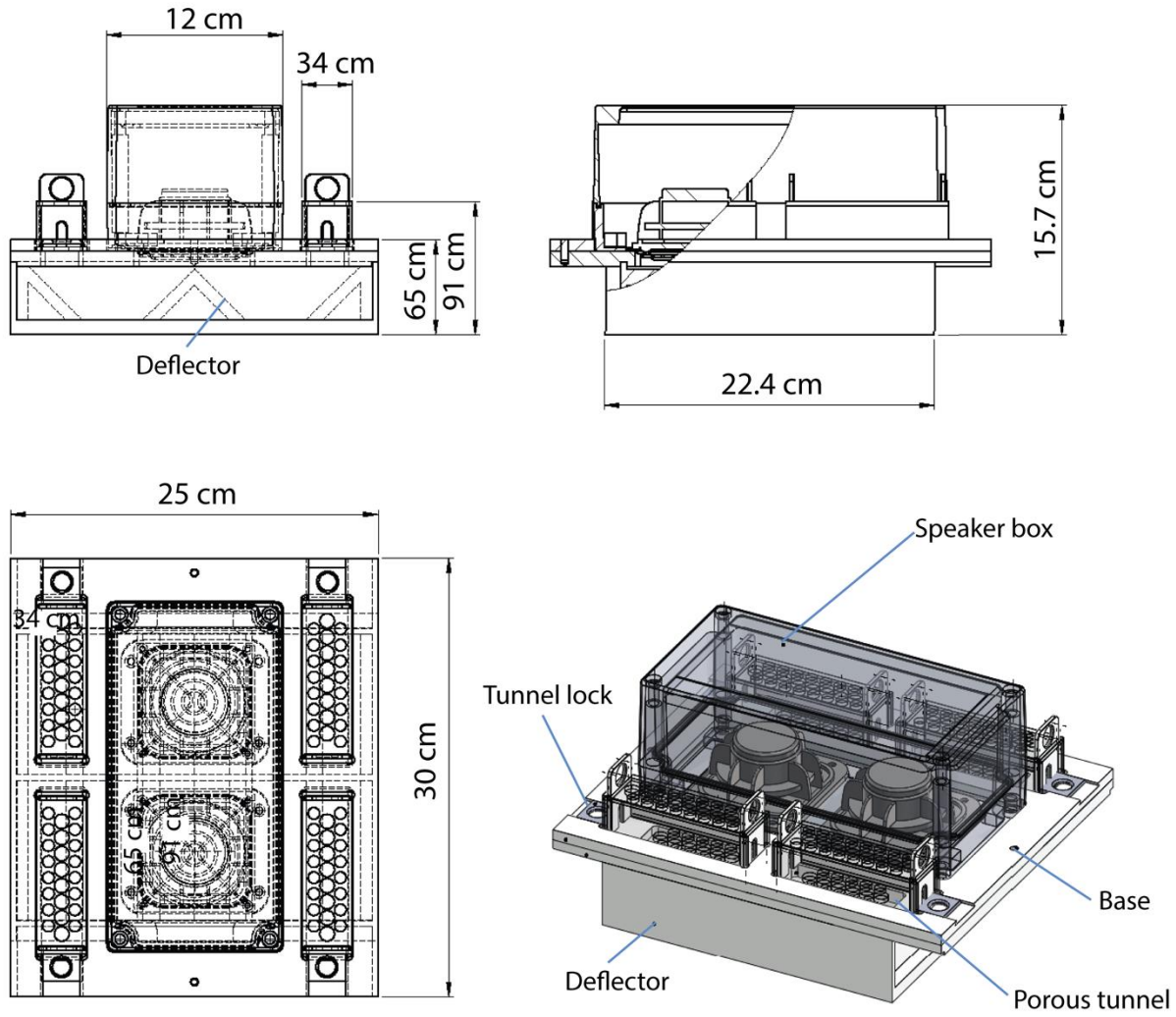

Figure S14. Three-dimensional and perspective views of the speaker setup for the in vivo study, with scale details. The deflector focuses the acoustic waves from loudspeakers onto the porous tunnel.

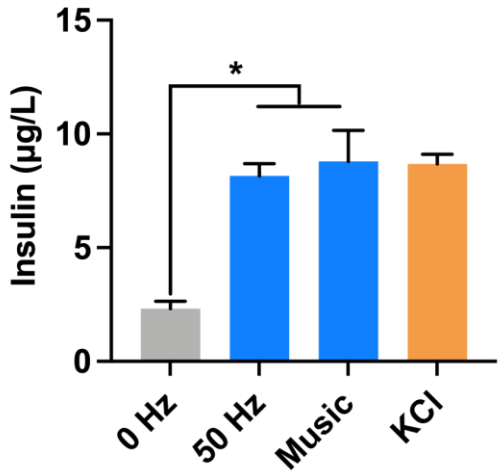

Figure S15. Alginate-encapsulated $MUSIC_{INS}$ stimulation at 50 Hz or "We Will Rock You" for 15 min. The statistical significance of the differences between the 50 Hz/music and 0 Hz groups was calculated using a two-tailed Mann-Whitney non-parametric test (n = 6). Data are means ± SEM. *P < 0.05.

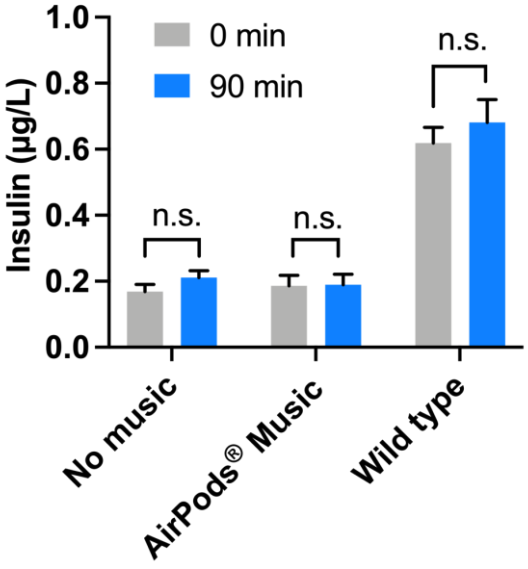

Figure S16. The $MUSIC_{INS}$ implanted type-1 diabetic mice were stimulated with "We Will Rock You" for 15 min via Apple AirPods®. Blood samples were collected at 90 min after stimulation. Type-1 diabetic mice without music stimulation were used as the negative control. Data are means ± SEM. The statistical significance of the differences between before stimulation and 90 min after stimulation for the three mouse groups was calculated using two-tailed Mann-Whitney non-parametric tests (n = 6). n.s. not significant.

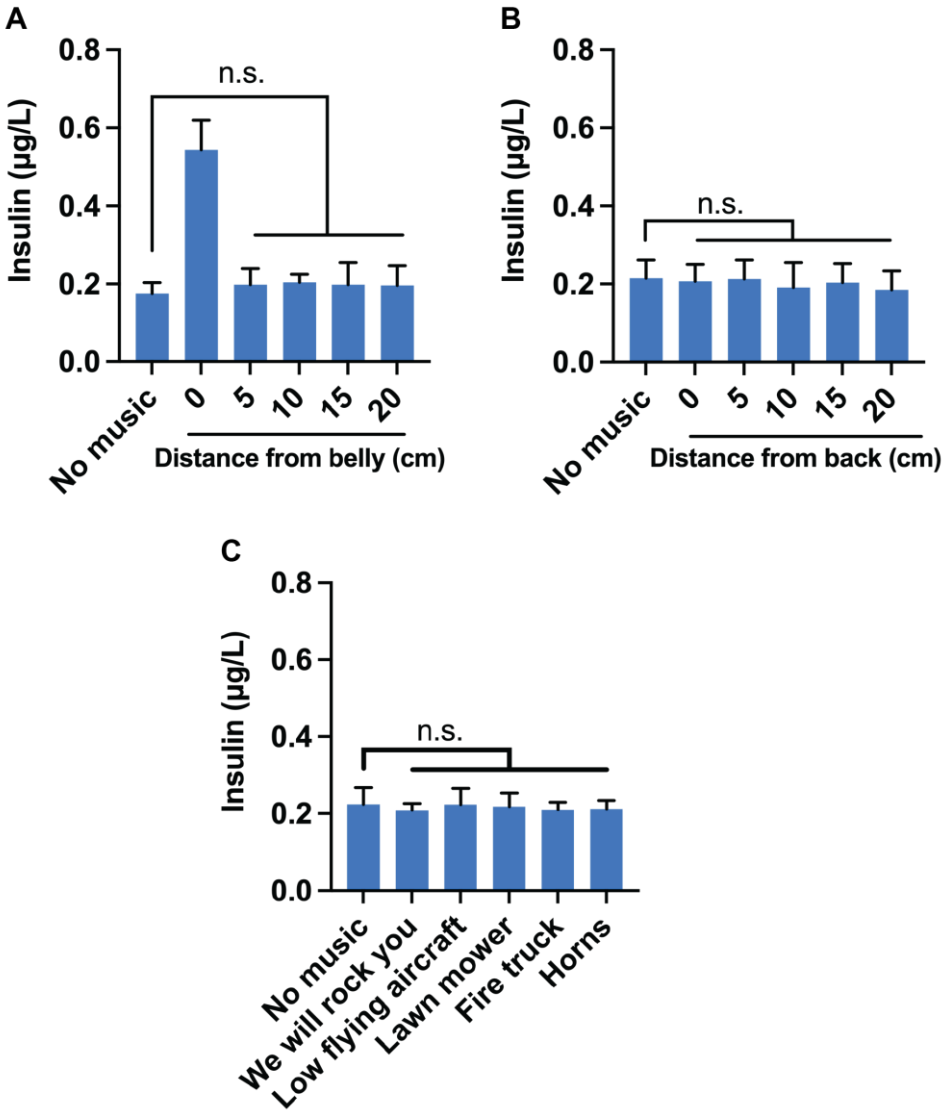

Figure S17. MUSIC$_{INS}$-implanted type-1 diabetic mice were exposed to music and various environmental noises from different distances and directions during 15 min via a portable loudspeaker. (A-B) Distance and direction dependence in the case of music exposure. Sound waves were directed from the loudspeaker to the belly (A) or the back (B) of the mice from different distances. The statistical analysis compared the "No music" group with the different distance groups. (C) The insulin secretion levels of mice exposed to loud environmental noises, delivered via the loudspeaker at the same level as the music, while walking normally in the cage. Blood samples were collected at 90 min after stimulation. The statistical analysis compared the "No music" group and the groups exposed to different types of environmental noise using two-tailed Mann-Whitney non-parametric tests (n = 5). Data are means ± SEM. n.s. not significant.

Table S1. Key plasmids used in this study.

Plasmid	Description and cloning strategy	Reference or Source
pcDNA3.1 (+)	Mammalian expression vector (P_{hCMV}-MCS-pA).	Life Technologies, CA
pCMV-MscL-PA	Vector for integration of two expression cassettes flanked by insertion and recognition sites of Sleeping Beauty transposase (SB). The first cassette contains P_{hCMV}-driven mammalian bacterial large conductance mechanosensitive ion channel (MscL). The second cassette comprises P_{RPBSA}-driven mRUBY fluorescent protein coupled to zeocin resistance marker (ZeoR) (ITR-P_{hCMV}-MscL-pA: P_{RPBSA}-mRUBY-P2A-ZeoR-pA-ITR)	Strittmatter et al. 2021
pCMV-MscS-PA	Vector for integration of two expression cassettes flanked by insertion and recognition sites of Sleeping Beauty transposase (SB). The first cassette contains P_{hCMV}-driven mammalian bacterial small conductance mechanosensitive ion channel (MscS). The second cassette comprises P_{RPBSA}-driven mRUBY fluorescent protein coupled to zeocin resistance marker (ZeoR) (ITR-P_{hCMV}-MscS-pA: P_{RPBSA} -mRUBY-P2A-ZeoR-pA-ITR)	Unpublished
pCMV-T7-SB100	Constitutive SB100X expression vector (P_{hCMV}-SB100X-pA) (Addgene no. 34879).	Mates et al. 2009
pJH49	Vector for stable integration expression cassettes flanked by insertion and recognition sites of Sleeping beauty transposase (SB). Cassette contains P_{RPBSA}-driven yellow florescent protein (YPet) couple to puromycin resistance marker (ITR-P_{RPBSA}-YPet-P2A-PuroR-pA-ITA)	Unpublished
pMD2.G	Constitutive VSV-G expression vector (P_{hCMV}-VSV-G-pA). (Addgene no. 12259).	Follenzi et al. 2002
pProinsulin-Nluc	Lentiviral vector for constitutive expression of Proinsulin-NanoLuc (LTR-P_{hCMV}-Proinsulin-NanoLuc-pA: P_{hPGK}-BlastR-pA-LTR). (Addgene no. 62057).	Burns et al. 2015
pTS2386	Constitutive mammalian GCaMP6s expression vector (P_{hCMV}-GCaMP6s-pA).	Unpublished
pTS391	Vector for stable integration of two expression cassettes flanked by insertion and recognition sites of Sleeping Beauty transposase (SB). Cassette one contains P_{hCMV}-driven mammalian Piezo1 (mPiezo1). Cassette two comprises P_{RPBSA}-driven blue fluorescent protein	Strittmatter et al. 2021

	(BFP) coupled to puromycin resistance marker (PuroR). (ITR-P_{hCMV}-mPiezo1-pA:P_{RPBSA}-BFP-p2a-PuroR-pA-ITA)	
psPAX2	Lentiviral packaging vector. (Addgene no. 12260)	Aichberger et al. 2005
pHZ010	SB100X-specific transposon containing a MscL channel couple with PuroR expression unit and a constitutive marker of mRUBY and ZeoR expression unit (ITR-P_{hCMV}-MscL-P2A-PuroR-pA:P_{RPBSA}-mRUBY-P2A-ZeoR-pA-ITR). P2A-PuroR was PCR-amplified from JH49 using oligonucleotides oHZ040 (5'- cagaataaccgctctgctagcAGTGGTGGTTCTGGTGG-3'), oHZ041 (5'-ctgatcagcgagctgaagcttTCAGGCACCGGGCTTGCG-3'), restricted with NheI/HindIII and cloned into the corresponding sites (NheI/HindIII) of pTS416.	This work
pHZ030	SB100X-specific transposon containing a MscS channel couple with PuroR expression unit and a constitutive marker of mRUBY and ZeoR expression unit (ITR-P_{hCMV}-MscS-P2A-PuroR-pA:P_{RPBSA}-mRUBY-P2A-ZeoR-pA-ITR). P2A-PuroR was PCR-amplified from JH49 using oligonucleotides oHZ040 (5'-cagaataaccgctctgctagcAGTGGTGGTTCTGGTGG-3'), oHZ041 (5'-ctgatcagcgagctgaagcttTCAGGCACCGGGCTTGCG-3'), restricted with NheI/HindIII and cloned into the corresponding sites (NheI/HindIII) of pTS414.	This work
pHZ031	SB100X-specific transposon containing a PIEZO1 channel couple with PuroR expression unit and a constitutive marker of mRUBY and ZeoR expression unit (ITR-P_{hCMV}-PIEZO1-P2A-PuroR-pA:P_{RPBSA}-mRUBY-P2A-ZeoR-pA-ITR). PIEZO1 was excised from pTS391 using EcoRI /NheI and cloned into the corresponding sites of EcoRI /NheI of pHZ010.	This work

Abbreviations: BFP, blue fluorescent protein; **BlastR**, blasticidin resistance gene; **GCaMP6s**, ultrasensitive protein calcium sensor; **ITR**, inverted terminal repeat of SB100X; **NanoLuc**, *Oplophorus gracilirostris* luciferase; **pA**, polyadenylation signal; **mRUBY**, monomeric red fluorescent reporter; **mPIEZO1**, mammalian Piezo1 mechanosensitive ion channel; **LTR**, long terminal repeat; **MCS**, multiple cloning site; **MscL**, bacterial large conductance mechanosensitive ion channel; **MscS**, bacterial small conductance mechanosensitive ion channel; **P2A**, porcine teschovirus-1 2A self-cleaving peptide; **PCR**, polymerase chain reaction; **P_{hCMV}**, human cytomegalovirus immediate early promoter; **P_{mPGK}**, mouse phosphoglycerate promoter; **Proinsulin-NanoLuc**, modified proinsulin with its C-peptide

replaced by NanoLuc; **P$_{RPBSA}$**, constitutive synthetic mammalian promoter; **PuroR**, puromycin resistance gene; **SB**, sleeping Beauty; **SB100X**, optimized Sleeping Beauty transposase; **VSV-G**, vesicular stomatitis virus protein G; **YPet**, yellow fluorescent reporter; **ZeoR**, zeocin resistance gene.

References

Aichberger, K. J., M. Mayerhofer, M. T. Krauth, A. Vales, R. Kondo, S. Derdak, W. F. Pickl, E. Selzer, M. Deininger, B. J. Druker, C. Sillaber, H. Esterbauer, and P. Valent. 2005. 'Low-level expression of proapoptotic Bcl-2-interacting mediator in leukemic cells in patients with chronic myeloid leukemia: role of BCR/ABL, characterization of underlying signaling pathways, and reexpression by novel pharmacologic compounds', *Cancer Res*, 65: 9436-44.

Burns, S. M., A. Vetere, D. Walpita, V. Dancik, C. Khodier, J. Perez, P. A. Clemons, B. K. Wagner, and D. Altshuler. 2015. 'High-throughput luminescent reporter of insulin secretion for discovering regulators of pancreatic Beta-cell function', *Cell Metab*, 21: 126-37.

Follenzi, A., G. Sabatino, A. Lombardo, C. Boccaccio, and L. Naldini. 2002. 'Efficient gene delivery and targeted expression to hepatocytes in vivo by improved lentiviral vectors', *Hum Gene Ther*, 13: 243-60.

Mates, L., M. K. Chuah, E. Belay, B. Jerchow, N. Manoj, A. Acosta-Sanchez, D. P. Grzela, A. Schmitt, K. Becker, J. Matrai, L. Ma, E. Samara-Kuko, C. Gysemans, D. Pryputniewicz, C. Miskey, B. Fletcher, T. VandenDriessche, Z. Ivics, and Z. Izsvak. 2009. 'Molecular evolution of a novel hyperactive Sleeping Beauty transposase enables robust stable gene transfer in vertebrates', *Nat Genet*, 41: 753-61.

Strittmatter, T., P. Argast, P. Buchman, K. Krawczyk, and M. Fussenegger. 2021. 'Control of gene expression in engineered mammalian cells with a programmable shear-stress inducer', *Biotechnol Bioeng*, 118: 4751-9.

Supplementary Movie Legends

Movie S1. Movie showing the changes of intracellular calcium concentration in cells transiently transfected with MscL and/or expressing the genetically encoded calcium sensor GCaMP6s. The cultures were continuously stimulated at 70 Hz and the calcium-mediated green fluorescence of GCaMP6s was recorded by time-lapse microscopy. Since the sound-stimulation causes vibration of the microscope, the movie is blurred. Therefore, the 70 Hz stimulation was switched off after second 6 of the movie.

Movie S2. Movie showing type-1 diabetic mice exposed to an acoustic stimulus of 60 dB (50 m/s^2) at 50 Hz in the speaker setup. Note that the mice are breathing normally and are not shaking in sync with the tunes as they “listen” to the music.

Movie S3. Movie showing type-1 diabetic mice listening to "We Will Rock You" in the speaker setup. Note that the body of the animals does not vibrate in sync with the tunes, suggesting that they are indeed "listening" to the music rather than "trembling" or “vibrating” to absorb the sound waves.

Movie S4. Movie showing type-1 diabetic mice listening to "We Will Rock You" via Apple AirPods®, which does not trigger insulin secretion.

Movie S5. Movie showing type-1 diabetic mice "listening" to “We Will Rock You” while moving freely around the loudspeaker. Since the sound waves were not constantly focused on the implanted cells, they were not stimulated and did not produce any insulin. This suggests that MUSIC control would not be activated in response to normal daily activities.

Movie S6. Movie showing type-1 diabetic mice listening to "We Will Rock You" while sitting on a portable loudspeaker. Note that the body of the animals does not vibrate in sync with the tunes, suggesting that they are indeed "listening" to the music rather than "trembling" or “vibrating” to absorb the sound waves.

Author contributions. H.Z. and M.F. designed the project; H.Z. performed all cell culture experiments; P.B. designed the speaker set-up; H.Z., S.X. and M.D.H. performed the animal experiments; H.Z., S.X., A.P.T. and M.F. designed the experiments and analyzed the results; H.Z., S.X., A.P.T. and M.F. wrote the manuscript.

Data and materials availability. The authors declare that all the data supporting the findings of this study are available within the paper and its supplementary materials. All materials and original plasmids listed in Supplementary Table S1 are available upon request.